Atmospheric Environment 246 (2021) 118079

Contents lists available at ScienceDirect

Atmospheric Environment

journal homepage: http://www.elsevier.com/locate/atmosenv

Simulation of secondary organic aerosol over the Yangtze River Delta region: The impacts from the emissions of intermediate volatility organic compounds and the SOA modeling framework

Ling Huang [a,b,1], Qian Wang [a,b,1], Yangjun Wang [a,b,**], Chris Emery [c], Ansheng Zhu [a,b], Yonghui Zhu [a,b], Sijia Yin [a,b], Greg Yarwood [c], Kun Zhang [a,b], Li Li [a,b,*]

[a] School of Environmental and Chemical Engineering, Shanghai University, Shanghai, 200444, China
[b] Key Laboratory of Organic Compound Pollution Control Engineering (MOE), Shanghai University, Shanghai, 200444, China
[c] Ramboll, Novato, 95955, California, USA

HIGHLIGHTS

- IVOCs emissions estimated by different methods differ by a factor of 2.
- Simulated SOA concentrations could be enhanced by IVOCs emissions.
- SOA modeling schemes have important influences on simulated SOA and the fraction of biogenic vs. anthropogenic sources.

ARTICLE INFO

Keywords:
Secondary organic aerosols (SOA)
Intermediate-volatility organic compounds (IVOC)
CAMx
Yangtze river delta

ABSTRACT

Secondary organic aerosols (SOA) are an important component of fine particulate matter ($PM_{2.5}$). However, photochemical models often have difficulty capturing the observed magnitudes of SOA due to uncertainties in precursor emissions and modeling approach. In this study, we conducted a modeling study of SOA in the Yangtze River Delta (YRD) region of China to investigate the impact of emissions of intermediate-volatility organic compounds (IVOC) and the SOA modeling schemes. IVOC emissions, which are important SOA precursors but are missing from most emission inventories, are estimated for the YRD region based on two methods. First, scaling IVOC from emissions of primary organic aerosols (POA) estimates 730 Gg with on-road and industry sectors being the main contributors. Second, scaling IVOC emissions using emission factors and activity data estimates 313 Gg, 57% lower than the first method, with industry and off-road sectors being the major contributors. A photochemical model simulation of SOA for July 2018, conducted using standard emission inventories for the YRD region, significantly underestimates SOA by 61% at the Dianshan Lake monitoring site (DSL). A series of simulations with two different SOA modeling schemes found that with the traditional two-product modeling framework, IVOC emissions enhance simulated SOA concentrations by 8%–27% at DSL and 5%–26% over the YRD region in July 2018. Increasing SOA mass yields from IVOC by a factor of five leads to better agreement with observations at the DSL site. Switching to the 1.5-Dimension Volatility Basis Set (VBS) approach increases simulated SOA by 76% at DSL but reduced POA concentration by 72%, leading to an overall decrease of organic aerosol (OA) by 12%. Unlike the two-product scheme where POA is entirely inert, the VBS scheme includes POA in the OA chemistry. The SOA:OA ratio and the anthropogenic-to-biogenic SOA ratio (ASOA:BSOA) also vary systematically with SOA modeling schemes suggesting that detailed measurements of SOA composition could further constrain modeling methods.

* Corresponding author. Key Laboratory of Organic Compound Pollution Control Engineering (MOE), Shanghai University, Shanghai, 200444, China.
** Corresponding author. School of Environmental and Chemical Engineering, Shanghai University, Shanghai, 200444, China.
E-mail addresses: yjwang326@shu.edu.cn (Y. Wang), lily@shu.edu.cn (L. Li).
[1] These authors contributed equally to this work.

https://doi.org/10.1016/j.atmosenv.2020.118079
Received 26 July 2020; Received in revised form 8 November 2020; Accepted 11 November 2020
Available online 14 November 2020

1. Introduction

Atmospheric fine particulate matter ($PM_{2.5}$, aerodynamic diameters less than 2.5 μm) impacts atmospheric visibility, human health, and climate change (Kampa et al., 2008; Liu et al., 2014; Pui et al., 2014; Xie et al., 2014). Organic aerosol (OA) is an important component of $PM_{2.5}$, accounting for 20–90% of total $PM_{2.5}$ mass (Zhang et al., 2007). OA is composed of both directly emitted, or primary, organic aerosol (POA) as well as secondary organic aerosol (SOA). SOA is generated via oxidation reactions involving precursor emissions of volatile organic compounds (VOC) that form condensable gases with varying vapor pressures, followed by gas-particle partitioning (Murphy et al., 2006). SOA represents an important part of OA (Guo et al., 2014; Huang et al., 2014; Sun et al., 2016), particularly in China where previous studies show that SOA accounts for 31–65% of OA in Shanghai and 30–76% in Beijing (Xu et al., 2015, 2018; Sun et al., 2016; Zhang et al., 2018). Compared with secondary inorganic aerosols (i.e. sulfate, nitrate, and ammonium), SOA precursors and formation mechanisms are much more complicated and less understood (Hallquist et al., 2009). Due to the inclusion of polar functional groups such as oxygen and nitrogen, SOA exhibits stronger solubility and hygroscopicity, and thus presents greater impacts on aerosol optical properties and health effects (Gao et al., 2019; Zheng et al., 2014).

SOA budgets in different regions of China have been estimated by three-dimensional photochemical air quality models (Lin et al., 2016; Li et al., 2019, 2020; J Li et al., 2019; Liu et al., 2020; Yao et al., 2020). In early years, SOA simulations were mostly conducted based on the "two-product" approach (Odum et al., 1996), such as the Secondary Organic Aerosol Processor (SOAP; Strader et al., 1999), which assumes that POA is non-volatile and unreactive, and each VOC precursor forms several product compounds that can coexist in the gas and aerosol phases based on their saturation concentration. However, experimental results have shown that POA is semi-volatile and can evaporate into the gaseous phase for further photochemical oxidation and therefore producing SOA (Robinson et al., 2007; Donahue et al., 2009). As a result, models based on the two-product approach largely underestimate SOA concentrations (e.g. Jiang et al., 2012; Fu et al., 2011; Meroni et al., 2017). To improve SOA simulations, Donahue et al. (2006) introduced the concept of the Volatility Basis Set (VBS), which provides a unified framework for gas-aerosol partitioning and chemical aging of both POA and SOA. Compared with the two-product approach, VBS is shown to significantly improve simulated SOA concentrations (e.g. Han et al., 2016; Meroni et al., 2017; Giani et al., 2019). For example, Lin et al. (2016) simulated SOA in Beijing with both the two-product and VBS schemes and found that the latter improved the average SOA concentration by 86%. Yao et al. (2020) simulated SOA with the traditional two-product approach, a 1-dimensional (1-D) VBS and a 1.5-dimensional (1.5-D) VBS within the Comprehensive Air quality Model with extensions (CAMx) in the Pearl River Delta (PRD) region, and found that 1-D VBS could better capture peak SOA concentrations while simulated annual average SOA concentrations increased by 63% relative to traditional SOA approaches.

In addition to improved SOA modeling schemes, inclusion of missing SOA precursors also leads to improved SOA simulations. Intermediate-volatility organic compounds (IVOC) are found to be important SOA precursors (Tkacik DS et al., 2012; Woody et al., 2014; Giani et al., 2019; Lannuque et al., 2019) and have significant impacts on SOA formation (Robinson et al., 2007 Jathar et al., 2017). IVOC are species with effective saturation concentration between 10^3 μg m^{-3} and 10^6 μg m^{-3}, which, for context, correspond to n-alkanes $C_{12} \sim C_{22}$ n-alkanes (Donahue et al., 2009; Presto et al., 2010). Many studies have found that adding IVOC emissions generally improved SOA simulation results (Couvidat et al., 2013; Hayes et al., 2015; Woody et al., 2016). For example, Zhao et al. (2016a) estimated IVOC emission based on IVOC: POA ratios and found that the contribution of IVOC emissions to SOA concentrations was about 50% in eastern China in 2010. Li et al. (2020) investigated the evolution and distribution of SOA over the Beijing-Tianjin-Hebei (BTH) region during the winter of 2014 and found that IVOC contributed 40% to SOA formation. However, IVOC emissions are usually not calculated or reported in conventional emission inventories, yet there are large uncertainties associated with emission rates when they are estimated (Xia et al., 2018; Lu et al., 2018; Sun et al., 2018; Wu et al., 2019).

The Yangtze River Delta (YRD) region, one of the three most developed city-clusters in China (including BTH and PRD), has experienced heavy haze pollution during the past decade (e.g. Lin et al., 2016; Sun et al., 2020; Liu et al., 2020). With tremendous efforts to mitigate air pollution over China, the overall air quality in YRD has greatly improved over the past few years (Ministry of Ecology and Environment of China, 2019). The contribution of OA to $PM_{2.5}$ in YRD exceeded 40% with SOA contributing up to 69% of OA during the haze event in January 2013 (Wang et al., 2009; Huang et al., 2014; Cheng et al., 2014; Chen et al., 2016), indicating that SOA is an important $PM_{2.5}$ component. To continuously reduce $PM_{2.5}$ concentrations in YRD, it is important to understand the spatial and temporal patterns of SOA concentrations. However, modeling studies of SOA in YRD are lacking (Liu et al., 2020). The most recent study by Liu et al. (2020) investigated source contributions of SOA during winter pollution episodes in YRD based on the Community Multiscale Air Quality (CMAQ) model. However, IVOC emissions were not considered in their study, which could lead to biased sectoral contributions to SOA formation to some extent.

In this study, we first developed a comprehensive IVOC emission inventory with high spatial and temporal resolution for the YRD region using two different methods. SOA concentrations were then simulated with the SOAP scheme as well as the 1.5-D VBS scheme within the CAMx (Ramboll, 2018) for the month of July 2018. Several sensitivity simulations examine the contribution of IVOC emissions to SOA and the influences of two different SOA modeling schemes over YRD. Results from this study provide useful information with respect to the spatial and temporal patterns of precursor emissions and SOA concentrations throughout YRD, which can further guide air pollution control in the future.

2. Methodologies

2.1. Development of IVOC emissions inventory

Previous studies estimated IVOC emissions either by applying a source-specific IVOC factors to POA emissions (Hodzic et al., 2010; Woody et al., 2015; Murohy et al., 2017) or to emissions of non-methane organic gases (NMOG, Jathar et al., 2014). Alternatively, several studies calculated IVOC emissions from directly-measured IVOC emission factors from different sources (Huang et al., 2018; Zhao et al., 2015, 2016b). In this study, we applied both the IVOC:POA ratio method (referred to here as the POA method) and the emission factor method (referred here as the EF method) to estimate IVOC emissions for the YRD region.

For the POA method, a wide range of ratios have been used in previous studies for different sources. For instance, Robison et al. (2007) and Hodzic et al. (2010) estimated total IVOC emissions by multiplying POA emissions by a factor of 1.5 regardless of emission sector. Depending on the fuel type, reported ratios of IVOC emissions to POA emissions from on-road and non-road sources range from 1.5 to 30.0 (Robinson et al., 2007; Zhao et al., 2016a). Most of the previous studies applied the ratio of 1.5 for industry, biomass burning (i.e. domestic combustion), cooking and other sources. Table 1 lists the IVOC:POA ratios adopted in this study.

Estimation of IVOC emission based on the EF method is shown in Eq. (1):

$$E_i = A_i \times EF_{IVOCs,i} \quad \text{Eq. (1)}$$

Table 1
IVOC:POA ratios employed in this study for different emission sectors.

Emission category	IVOCs/POAs	References
Industry	1.5	Robinson et al. (2007)
Biomass burning	1.5	Zhao et al. (2016a)
Cooking	1.5	Robinson et al. (2007)
Dust	1.5	Robinson et al. (2007)
Residential combustion	1.5	Robinson et al. (2007)
On-road	8	Zhao et al. (2015)
Off-road	8	Zhao et al. (2016a)

where E_i represents IVOC emissions from source i; EF_{IVOC} represents the source-specific IVOC emission factor; A_i represents the local activity data for different sources. Due to data availability, IVOC emissions from on-road, residential combustion and biomass burning were calculated using the EF method. Activity data (for example, vehicle volume, road length, off-road mobile volume, straw burned and coal volume, etc.) were collected from the 2018 statistical yearbooks for 41 cities in the YRD region. IVOC emission factors for on-road vehicles were obtained from Zhao et al. (2015, 2016b, shown in Table S1) and emission factors for other sources are listed in Table S2.

2.2. Model configuration

An integrated modeling system comprising the Weather Research and Forecasting (WRF) model version 3.40 and the CAMx version 6.50 photochemical grid model (Ramboll, 2018) were used to simulate SOA for the YRD region. WRF physics settings are listed in Table S3. The CAMx configuration included the Carbon Bond 6 (CB6) photochemical gas-phase mechanism (Yarwood et al., 2010), the static two-mode coarse/fine (CF) PM chemistry option with the ISORROPIA (Nenes et al., 1998) inorganic gas-aerosol partitioning scheme, Zhang dry deposition option (Zhang et al., 2003) and wet deposition. The organic PM chemistry methods employed in this study are described below. Three nested domains were used as shown in Fig. 1. Domain 1 (D01) covers most of China, Japan, Korean Peninsula, parts of India, and southeast Asia with a grid spacing of 36 km; Domain 2 (D02) covers the eastern part of China with 12 km grid spacing; the inner domain (D03) covers the YRD region (Shanghai, Jiangsu, Zhejiang, Anhui provinces) and parts of surrounding areas with a grid spacing of 4 km. Boundary conditions (BC) and initial conditions (IC) for D01 were extracted from the Model for Ozone and Related chemical Tracers (MOZART) global chemical model (Emmons et al., 2010) using CAMx pre-processing software. The simulation period of July 2018 included a 5-day spin-up period to mitigate the impact of initial conditions. Anthropogenic emissions outside the YRD region were based on the multi-resolution emission inventory for China (MEIC, http://www.meicmodel.org/). The emission inventory for the YRD region was locally developed (Huang et al., 2011) with activity data updated to year 2017. Anthropogenic emissions were prepared for modeling via the Sparse Matrix Operator Kernel Emissions (SMOKE) processing system (Houyoux et al., 2000). Biogenic emissions were generated using by an updated version of the Model of Emissions of Gases and Aerosols from Nature (MEGAN, version 3.0, http://aqrp.ceer.utexas.edu/projects.cfm) along with metrological data generated by WRF.

CAMx provides two modeling schemes for SOA chemistry: the SOAP scheme (Strader et al., 1999) and the 1.5-D VBS scheme (Koo et al., 2014). The former SOAP treats POA as non-volatile and includes species that do not undergo further chemical reactions and consist of two parts: gas-phase oxidation of anthropogenic and biogenic aromatic precursors forming condensable gases (CG) with gas-aerosol partitioning equilibrium distribution for forming SOA (Ramboll, 2018).

The latter VBS considers the volatility of POA and multiple generations of SOA, and has evolved from a 1-D to 1.5-D scheme (Donahue et al., 2006, 2011, 2012; Koo et al., 2014). In 1-D VBS, organic compounds are grouped only according to volatility and could not describe varying degrees of oxidation. The 2-D VBS groups organic compounds based on oxidation state and volatility but incurs high computation cost. 1.5-D VBS efficiently combines the simplicity of 1-D treatment of volatility with a representation of OA oxidation state (Koo et al., 2014). In terms of IVOC oxidation, SOAP scheme does not differentiate among different sources of IVOC emissions while VBS scheme does. In the former scheme, IVOC is oxidized by OH/HO_2 radical and NO to generate more-volatile, less-volatile and non-volatile products and the mass yields for each product is NOx-dependent (Ramboll, 2018). In VBS scheme, IVOC is oxidized only by OH radical with a rate constant of 4×10^{-11} cm^3 $molecules^{-1}$ s^{-1} and the mass yields is also NOx-dependent.

2.3. Simulation scenarios

In order to evaluate the impacts of IVOC emissions and SOA modeling framework on simulated SOA over the YRD region, five scenarios were conducted (Table 2). The BASE scenario was conducted without IVOC emissions, while the other four scenarios added IVOC

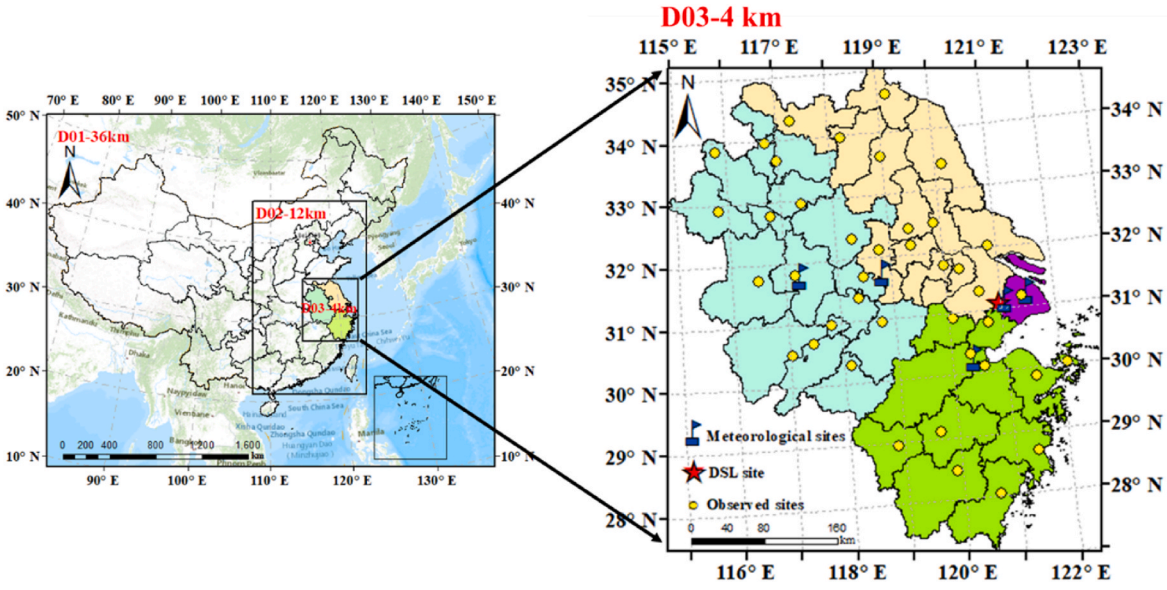

Fig. 1. CAMx modeling domains.

Table 2
CAMx simulation scenarios.

Scenarios	SOA chemistry	IVOC emissions	SOA mass yields from IVOCs
BASE	SOAP	/	default
SCEN1	SOAP	POA + EF methods	default
SCEN2	SOAP	POA method	default
SCEN3	SOAP	POA method	default × 5
SCEN4	1.5-D VBS	POA + EF methods	default

emissions. SCEN1 employed IVOC emissions estimated by the combination of both POA and EF methods (i.e. the POA method is used for industry, cooking, dust and off-road, and the EF method is used for on-road, biomass burning and residential combustion) while SCEN2 and SCEN4 used the POA method only (i.e. the POA method is used for all sources). Since SOA yields from IVOC are associated with large uncertainties (Chan et al., 2009; Stockwell et al., 2015; Zhao et al., 2016b; Hodzic et al., 2016; Ma et al., 2017; Qi et al., 2019), SCEN3 scaled the SOA mass yields by a factor of 5 to investigate sensitivity on top of SCEN2. For BASE and SCEN1 through SCEN3, the SOAP framework was used while for SCEN4 the 1.5-D VBS modeling framework was used.

2.4. Observed data

Hourly observed concentrations of $PM_{2.5}$, PM_{10}, SO_2, NO_2, and O_3 from July 1 to 31, 2018 at 41 monitoring sites over the YRD region (Fig. 1) were used for model validation. In addition, hourly observed data for organic carbon (OC) and elemental carbon (EC) over July 2018 at the Qingpu Dianshan Lake site (DSL site; 31.0935°N, 120.978°E, Fig. 1) was used for the validation of modeled OC and EC. Because SOA observations are not available, a direct comparison of modeled SOA with observations is not possible. Nevertheless, the observed OC and EC provide constraint for the total amount of carbon, and the ratio of the two is an indicator of the extent of secondary organic aerosol formation. At the same time, the observed SOA was estimated based on a relatively simple method for preliminary comparison with simulated SOA. Secondary organic carbon (SOC) was calculated from OC based on the minimum OC/EC ratio method (Castro et al., 1999; Cao et al., 2004). Fig. S1 shows the concentration of OC and EC and the OC/EC ratios for July at the DSL site. Based on these data, the $(OC/EC)_{min}$ of 1.0 was used in this study. Note that OC includes only mass of carbon, whereas OA includes all mass associated with organic aerosols (carbon, oxygen, hydrogen, etc.). Therefore, OA derived from CAMx must be converted to OC. An OA:OC ratio of 1.6 was used to convert simulated SOA for SOAP scheme (Feng et al., 2009); for VBS scheme, different OA:OC ratios for different OA sources and different volatility bins were used according to Koo et al. (2014) (Table S4). Observed hourly temperature (T), wind speed (WS), and relative humidity (RH) from Shanghai (Qingpu and Pudong), Hangzhou, Nanjing and Hefei were used for WRF evaluation (Fig. 1). The meteorological data were obtained from National Data Center of the Chinese Meteorology Agency (http://data.cma.cn/).

3. Results and discussions

3.1. Estimated IVOC emissions for the YRD region

Based on the POA method, total IVOC emissions in 2017 were estimated at 730 Gg, while IVOC emissions calculated by the EF method were 313 Gg, about half the value estimated by POA method (Table 3). Fig. 2 shows the total IVOC emissions at the provincial level based on these two methods. Anhui province has the largest IVOC emissions (124 Gg by EF method ~ 281 Gg by POA method), followed by Jiangsu (115 Gg ~ 259 Gg), Zhejiang (60 Gg–148 Gg) and Shanghai (13 Gg ~ 42 Gg). According to the IVOC emission inventory estimated by Liu et al. (2017), emission from vehicular sources in 2010 was 29 Gg for the YRD region, which is 1.8 times higher than the results by EF method but much lower than the results by POA method in our study.

Based on the POA method, on-road emissions were the largest IVOC contributor, accounting for 36.1% of the total, followed by industry (21.4%), biomass burning (13.1%), residential combustion (12.4%), and off-road machinery (10.2%). IVOC emissions from dust and cooking are relatively small (together less than 10%). For the EF method, industry was the largest IVOC contributor at 49.9%, followed by off-road (23.8%), and dust (12.0%). On-road emissions only accounted for 5.1% in the EF method in contrast to 36.1% in the POA method. Emissions from biomass burning, residential combustion and on-road sources in the POA method were respectively 6.4 times, 69.5 times and 16.5 times higher than those in EF method. The source contribution of IVOC emissions based on the POA method was similar to the results reported by Wu et al. (2019) for the PRD region, where the largest contributor of S/IVOC emissions was also on-road (41.6%), followed by industry (35.4%), and dust (14.5%).

The spatial distribution of total IVOC emissions estimated from both methods is shown by Fig. 3. IVOC emissions from individual source categories are shown in Fig. S2. For the POA method, the spatial distributions of total IVOC emissions over the YRD region were roughly consistent with the distribution of on-road and industrial sources. A large number of IVOC emissions associated with biomass burning (Fig. S2a) were found in Anhui and north of Jiangsu. IVOC emissions from dust sources in cities like Shanghai, Hefei, Ningbo and Xuzhou were high due to heavy traffic and accelerating urbanization processes (Fig. S2c). High industrial emissions of IVOC were mainly concentrated in the north of Anhui province, southern part of Jiangsu province (Suzhou-Wuxi-Changzhou) and Shanghai (Fig. S2g). The spatial distribution of IVOC emissions estimated based on the EF method were similar to the POA method except the magnitudes are much smaller.

The estimation of IVOCs emissions is associated with large uncertainties. This is demonstrated by the substantial difference of IVOCs emissions estimated based on two different methods. One important reason for this large difference is due to the fact that for most of the emission sources, the emission factor of IVOCs and the emission factor of POA were not measured simultaneously, except for the on-road sector where the emission factors for both POA and IVOCs were measured under the same conditions and the IVOC emission factor is estimated about 8 times that of POA (Zhao et al., 2015, 2016b). For other emission

Table 3
Estimated IVOC emission in the YRD region for year 2017.

Emission category	POA method		EF method		POA/EF method ratio
	IVOCs (Gg)	Contribution (%)	IVOCs (Gg)	Contribution (%)	
Industry	156.1	21.4	156.1	49.9	1.0
Residential combustion	90.3	12.4	1.3	0.4	69.5
On-road	263.6	36.1	16.0	5.1	16.5
Off-road	74.4	10.2	74.4	23.8	1.0
Dust	37.7	5.2	37.7	12.0	1.0
Biomass burning	95.6	13.1	15.0	4.8	6.4
Cooking	12.4	1.7	12.4	4.0	1.0
Total	730.1	100.0	312.9	100.0	2.3

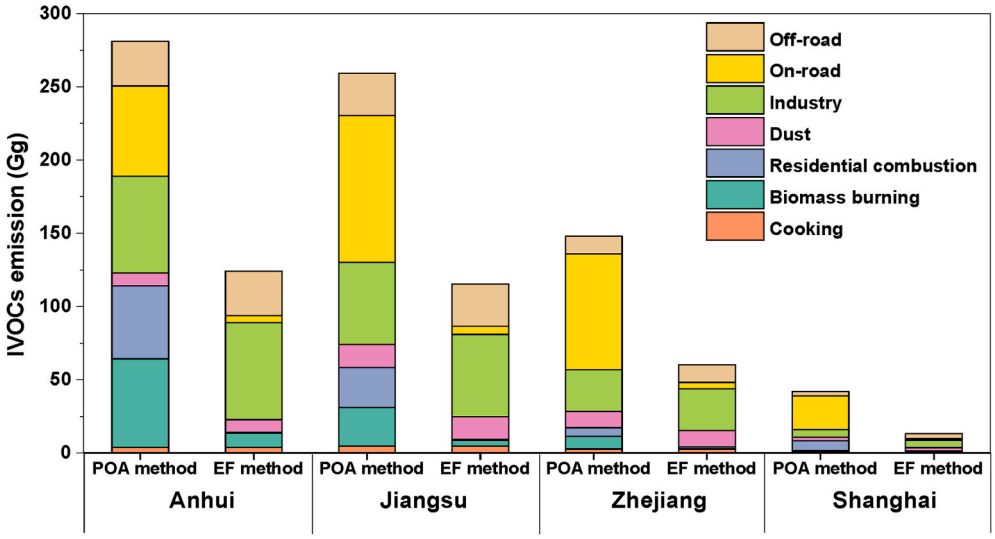

Fig. 2. IVOC emissions and proportions of different sources in the YRD region.

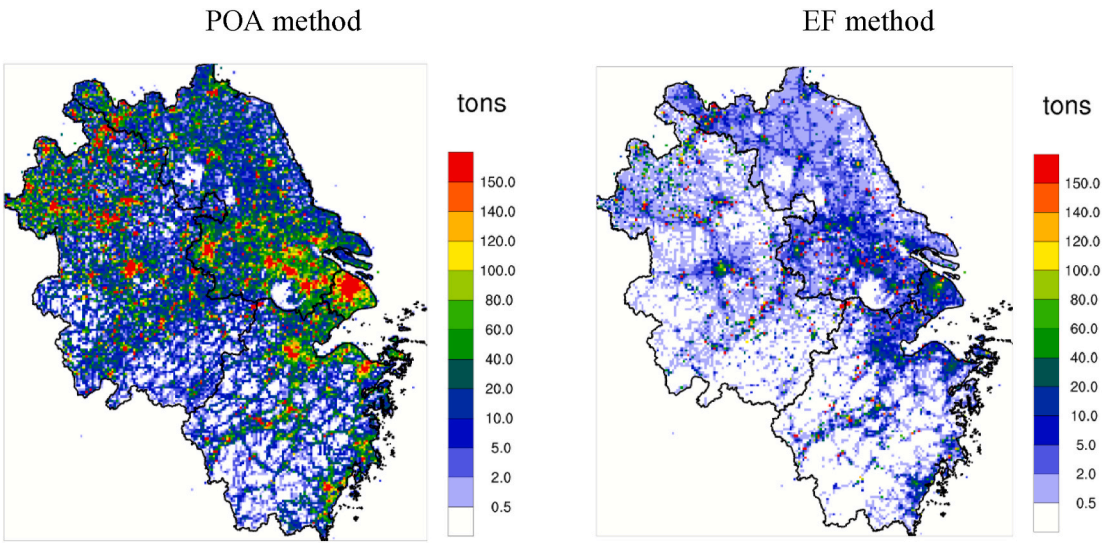

Fig. 3. Spatial distributions of total IVOC emissions from POA and EF methods.

sources where both the EF and POA method is applied (e.g. residential combustion), IVOCs emission factor is obtained from specific measurements studies whereas POA emissions are estimated based on the emission profile of $PM_{2.5}$. On top of that, the factor of 1.5 used for scaling IVOCs emissions based on POA is subjected to large uncertainties (Robinson et al., 2007; Zhao et al., 2016a). Future studies that directly measure IVOCs emissions from sources are needed to constrain the estimation of IVOCs emissions. We estimated uncertainties associated with IVOC emissions based on the Monte Carlo method. For the POA method, the probability distribution coefficients for different sources were based on the reliability of the local data with coefficients adopted from Wu et al. (2019) (Table S5). Based on our calculation, the uncertainty of total IVOC emissions over all source sectors in the YRD region during 2017 ranges from −36% to 386% at the 95% confidence interval, which is mainly contributed by uncertainties associated with emissions from off-road, dust and cooking. Since some uncertainty coefficients were not available for the EF method, we made some assumptions based on the reliability of the source data and obtained an uncertainty from 45% to 610% for IVOC emissions (Table S6).

3.2. *BASE model evaluation*

Table S7 summarizes meteorological performance statistics for simulated hourly T, WS, and RH during July 2018 at selected sites in Shanghai (Qingpu and Pudong site), Hangzhou, Nanjing, and Hefei (time series are included in Fig. S3). We applied commonly used statistical indicators including Index of Agreement (IOA), Mean Bias (MB) and Normalized Mean Bias (NMB) to evaluate model performance. In general, the model adequately captured the temporal variations of observed T and RH with IOA higher than 0.80 (except Hefei with IOA for WS and RH of 0.60 and 0.67, respectively). NMB for T was within −0.1%–0.5%, RH ranged −20.4% to −1.0%, and WS ranged −12.9%–33.2%. In summary, the meteorological simulations reasonably characterized weather conditions during July 2018 to support CAMx simulations.

Fig. S4 shows the spatial distribution of monthly average concentrations of $PM_{2.5}$, SO_2, NO_2 and O_3 over the YRD region during the simulation period. In general, the model tended to overestimate $PM_{2.5}$ and NO_2 concentrations, especially over Suzhou-Wuxi-Changzhou region. Observed $PM_{2.5}$ concentration generally showed a decreasing trend from north to south, which was captured by the model. For sites

located in northern Anhui, northern Jiangsu, and southern Zhejiang province, the simulation showed good agreement with observations, while in southern Anhui, southern Jiangsu, and northern Zhejiang province, the model overestimated $PM_{2.5}$. Table S8 shows the MB and NMB of $PM_{2.5}$ for selected monitoring sites over the YRD region. We also collected OC and EC observations reported for cities over the YRD region to show that our simulated OC concentrations are generally in the same order of magnitude with reported values in the literature while EC concentrations are lower (Table S9).

Fig. S5 depicts $PM_{2.5}$ daily time series for the DSL site over July 2018 while Table 4 summarizes statistical results for several chemical species. Overall, the model adequately captured the temporal variation of daily $PM_{2.5}$ and O_3 with IOA above 0.54 and 0.81, respectively. The model tended to underestimate $PM_{2.5}$ and NO_2 but overestimated O_3, SO_2 and PM_{10}. For carbonaceous aerosol, EC and OC were underestimated with NMB of −27% and −32% and underestimations of OC are usually associated with underestimation of SOA (Liu et al., 2020).

3.3. Simulated SOA at DSL site

In this section, we illustrate how the model simulated SOA concentrations at the DSL site with different model configurations. The time series of observed and simulated daily SOA concentrations are shown in Fig. 4 to demonstrate the model's capability of capturing the temporal variations (similar plots for OC and EC are shown in Fig. S6). Scatter plots of observed vs. modeled SOA, OA and EC concentrations are presented in Fig. 5.

As shown by Fig. 4, the model was able to capture day-to-day variations of SOA at the DSL site with noticeable peaks on July 25th. However, the model under predicted the magnitude of SOA concentrations: the observed monthly average SOA concentration (SOA_{avg}) was 3.7 μg m^{-3} while in the BASE scenario, the model predicted only 1.4 μg m^{-3}, an underestimation of 61.0%. The SOA:OA ratio based on observations was 0.67 (suggesting more secondary than primary organic aerosols) as opposed to only 0.36 in the BASE scenario. During July 24th to July 31st (referred as the episodic period, EP), the average observed SOA concentration was 6.2 μg m^{-3} (70.9% higher than July averaged concentrations); maximum hourly concentrations reached 26.1 μg m^{-3} (at 11:00 local time on July 26th), constituting 25.3% of $PM_{2.5}$ at this specific hour. For the EP, the BASE scenario estimated SOA concentration of only 2.4 μg m^{-3}, an underestimation of 61.2%. These results suggest that the traditional two-product scheme significantly underestimated the magnitude of observed SOA and the fact that underpredictions do not only occur during the EP indicates that a systematic underprediction exists. Observed EC concentration exhibits sharp increase during EP (Fig. S6), which might be due to sudden fluctuation of emissions that are not captured by the emission inventory.

3.3.1. The impact of IVOC emissions

IVOC emissions estimated by different methods were incorporated into SCEN1 and SCEN2, respectively, to investigate their contribution to SOA formation. With IVOC emissions, simulated SOA showed improvements over the BASE scenario, especially for SCEN2 when IVOC emissions were larger: SOA_{avg} in SCEN1 and SCEN2 was 1.5 μg m^{-3} and 1.8 μg m^{-3}, respectively, which increased by 7.9% and 26.8% compared to the BASE scenario. However, large SOA underestimations still existed with NMB of −58% and −51%, respectively (Fig. 5). In terms of SOA:OA (Fig. 6), adding IVOC emissions led to higher values over the BASE scenario in July 2018 at DSL site. This improvement is also evident during the EP: compared with the BASE scenario, the SOA_{avg} during the EP increased by 6.5% and 25.9% when IVOC emissions were added.

Simulated OA concentrations in SCEN1 were similar to the BASE scenario (Fig. 5), while SCEN2 showed slight improvement over the BASE scenario with increases of 19.0%. Interestingly, simulated EC concentrations were expected to remain constant under these different scenarios since it is treated as inert in CAMx using SOAP. However, the average EC concentration increased from 0.8 μg m^{-3} in the BASE scenario to 0.9 μg m^{-3} in SCEN2 (Fig. 5), representing an increase by 12.5%. This is likely attributable to changes in removal of EC via deposition. In CAMx, $PM_{2.5}$ is treated as an internal mixture and all $PM_{2.5}$ components share a single value of deposition velocity. This deposition velocity is dependent on the density and hygroscopicity of $PM_{2.5}$. It is likely that the increase of SOA in SCEN2 changes the overall deposition velocity that affects the removal of EC, whereas in SCEN1 the increase in SOA was much weaker and deposition rates were less affected.

Table 4
Statistics of BASE case model performance at DSL site.

Species	Observation (μg·m^{-3})	Model (μg·m^{-3})	MB	NMB	IOA
O_3	62.1	85.0	23.0	40%	0.81
NO_2	23.4	20.8	−2.6	−11%	0.61
SO_2	5.4	5.1	−0.3	−5%	0.44
PM_{10}	31.7	30.2	−1.5	−5%	0.46
$PM_{2.5}$	25.4	16.3	−9.1	−36%	0.54
EC	1.1	0.8	−0.3	−27%	0.54
OC	3.4	2.3	−1.1	−32%	0.55
OC:EC	3.4	3.0	−0.4	−13%	0.41

3.3.2. The impact of SOA mass yields

Given that adding IVOC emissions still underestimated SOA concentrations at the DSL site, and that large uncertainties exist with SOA yields from IVOC (Cappa et al., 2016; Ma et al., 2017; Qi et al., 2019), we conducted a third scenario (SCEN3) with IVOC emissions same as SCEN2 but with higher SOA mass yields by a factor of 5 (see Table S10). In fact, we conducted two more sensitivity studies where SOA yields were increased by 2 and 10 times; the former led to slight increases in SOA while the latter generated too much SOA. Results from SCEN3 showed that simulated SOA concentrations were significantly improved compared with previous scenarios: SOA_{avg} for SCEN3 increased by 135.8% and 85.9% compared with BASE and SCEN2, respectively. This increase led to much better agreement with observations at the DSL site where NMB and MB were only −8% and −0.3, respectively, and IOA increased to 0.79. During the EP, SOA_{avg} simulated in SCEN3 was 128.8% higher than BASE with an under estimation of only 10%.

With respect to OA and SOA:OA ratio, SCEN3 performed much closer to observed values in July 2018 at DSL site. Predicted OA in SCEN3 was 8.9% higher than observed due to the large increase in SOA. The SOA:OA ratio was around 0.57, slightly lower than observed. It is possible that POA emissions were overestimated in our study, which may have led to under estimated SOA:OA ratio but slightly over estimated OA concentrations. Nevertheless, these results from SCEN3 suggest that simulated SOA is sensitive to assumed mass yields from IVOC and further constraints from experimental studies are needed.

3.3.3. The impact of SOAs modeling scheme

To investigate the impact of an alternative OA treatment on simulated SOA concentrations, a fourth scenario (SCEN4) was conducted that utilized the 1.5-D VBS scheme while using IVOC emissions based on the EF method (i.e. same as SCEN1). Monthly SOA_{avg} simulated by the VBS scheme was 2.7 μg m^{-3}, 75.6% higher than the SOAP scheme in SCEN1. The NMB for simulated SOA was reduced from −58% in SCEN1 to −26% in SCEN4 and IOA increased from 0.53 to 0.78. During the EP, SOA_{avg} with the VBS scheme increased by 109.3% over the SOAP scheme. In terms of the SOA:OA ratio, VBS gave the highest value among all scenarios with an averaged ratio of 0.70 in July 2018 at DSL site, which is slightly higher than the observed value. The maximum simulated SOA:OA ratio reached 0.94, reflecting the multi-aging features of VBS over SOAP (no aging). During the EP, averaged SOA simulated by the VBS scheme was 5.4 μg m^{-3} with a SOA:OA ratio of 0.79.

However, VBS scheme reduced model performance for total OA compared to the SOAP scheme at the DSL site. The estimated OA_{avg} in

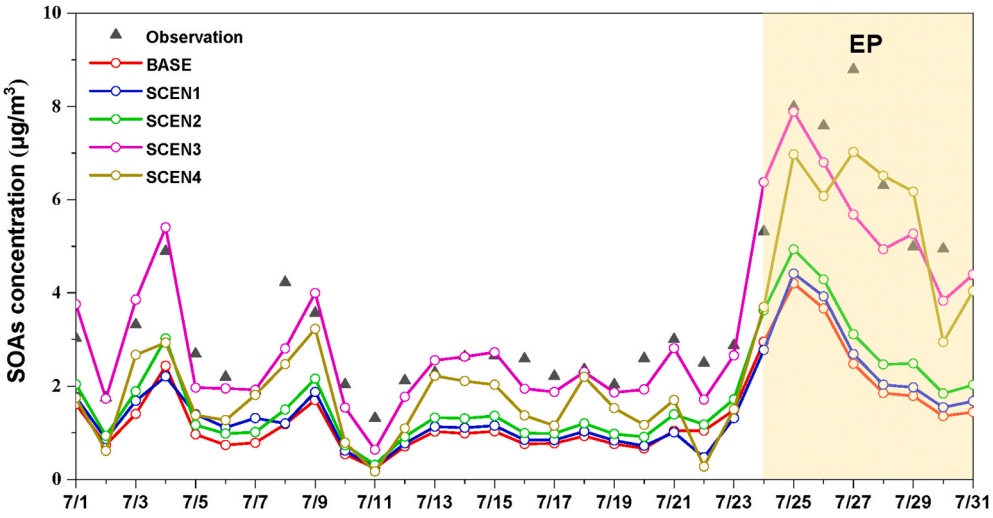

Fig. 4. Daily time series of observed and simulated SOA concentrations over July 2018 at the DSL site.

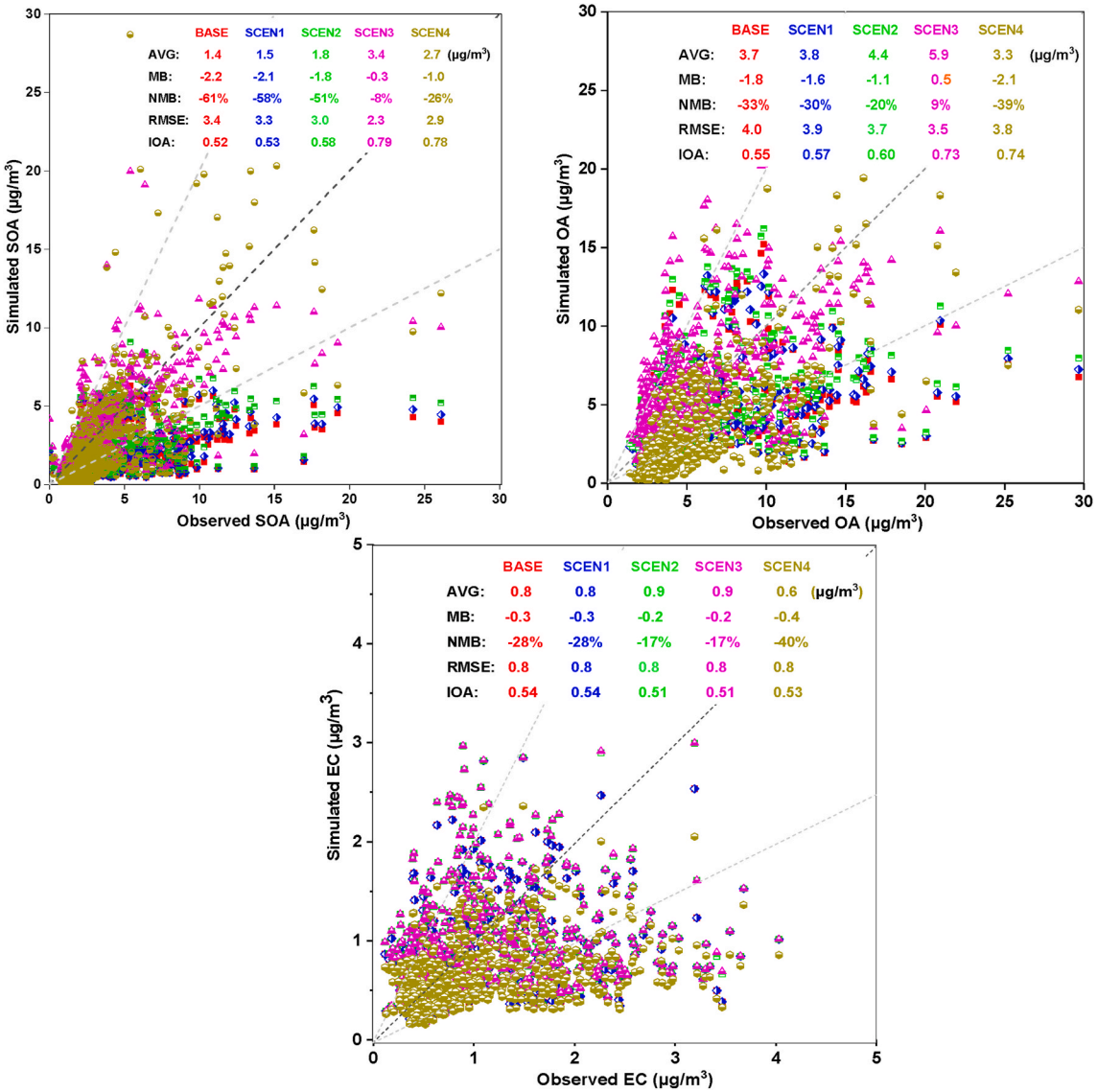

Fig. 5. Scatter plots of simulated and observed SOA (top left), OA (top right) and EC (bottom) concentrations from different model scenarios at the DSL site.

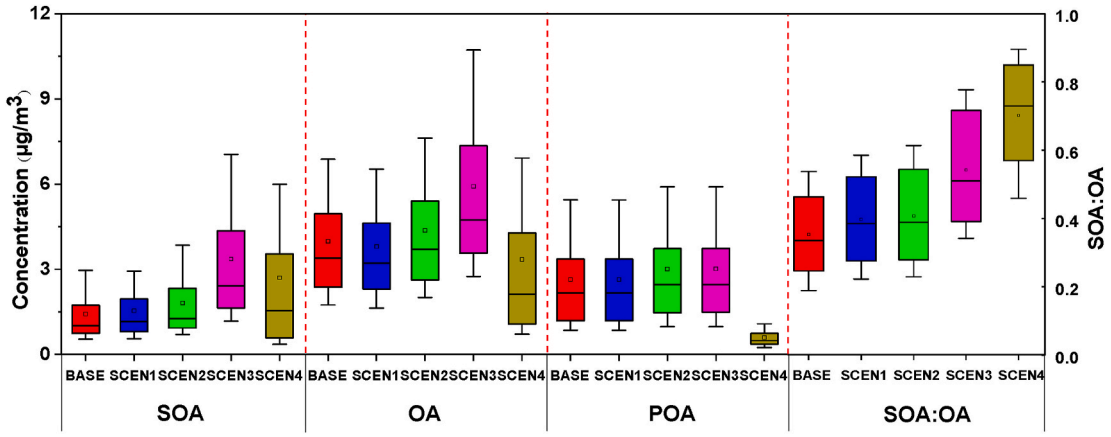

Fig. 6. Boxplots of SOA, OA, POA and SOA:OA in different model scenario at the DSL site (Whiskers below and above the boxes are the 10th and 90th percentiles; lower and upper boundaries of boxes are the 25th and 75th percentiles; lines and circles are the median and mean values, respectively).

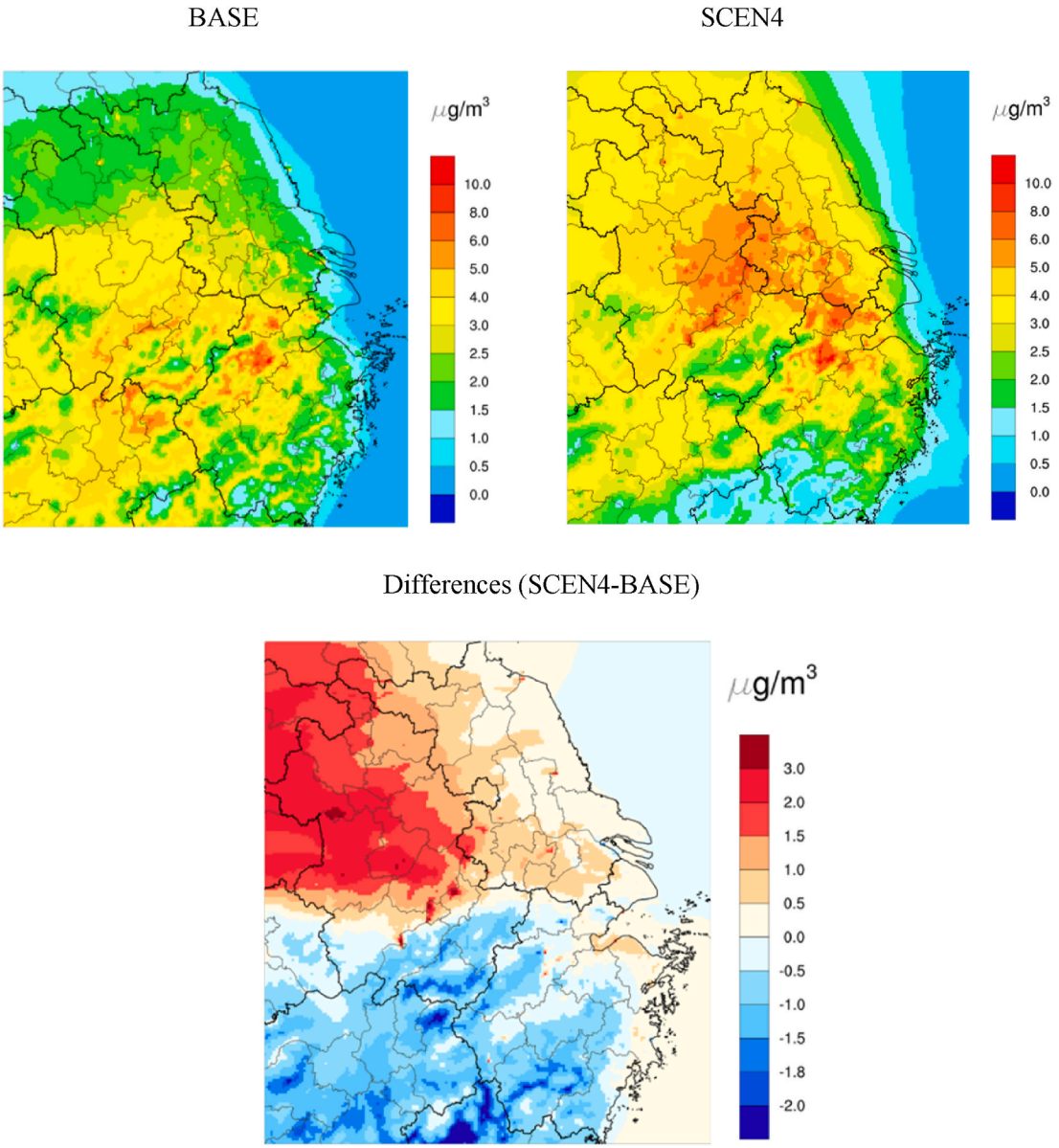

Fig. 7. Spatial distributions of monthly-average SOA in the BASE and SCEN4 scenario (top) and differences between the two (bottom).

SCEN4 was 3.3 μg m^{-3}, the lowest among all scenarios (even lower than BASE). Simulated OA was 38.5% lower than observation; this decrease was related to the treatment of POA as a semi-volatile species in VBS that exceeds the increase of SOA concentration due to additional formation and aging from the gas-phase precursors. At the DSL site, averaged POA concentration decreased from 2.6 μg m^{-3} in the BASE scenario to only 0.6 μg m^{-3} in SCEN4, which outcompeted the increase associated with SOA. It is obviously that the concentrations of POA in SCEN4 are much lower than other scenarios (Fig. 6). Another possibility that could partially explain the decrease in OA is again related to changes in the deposition velocity.

Results presented so far suggest that adding IVOC emissions could increase model simulated SOA concentrations by 7.9%–135.8%, depending on the magnitudes of those emissions as well as the SOA mass yields within the model, both of which are subjected to large uncertainties and need further constraints. The choice of SOA modeling scheme also exhibits significant impacts on simulated SOA concentrations, and more to the fraction of SOA that comprises total OAs due to different treatments of POA. At the DSL site, SOA simulated by the VBS scheme was 75.6% higher than the SOAP scheme whereas POA was 71.6% less, leading to an overall 16.0% lower OA in VBS scheme in July 2018. Other source of uncertainties associated with SOA includes its photolytic loss recently implemented in CAMx, which is also associated with significant uncertainties by orders of magnitudes (Henry and Donahue, 2012).

3.4. Spatial distribution of SOA over the YRD region

In the BASE scenario, domain-averaged SOA concentration was 1.4 μg·m^{-3} with high values (maximum of 11.4 μg·m^{-3}) over the boundary between southern Anhui and northern Zhejiang provinces (Fig. 7). In SCEN1 through SCEN3, where either IVOC emissions were added and/or SOA mass yields were boosted, simulated SOA concentrations showed ubiquitous increases over the entire domain (Fig. S7). The increase in average SOA ranged from 0.1 to 1.4 μg·m^{-3}, depending on the magnitude of IVOC emissions as well as the mass yields. The spatial patterns of SOA in SCEN1 and SCEN2 did not differ much from the BASE scenario. In SCEN3, maximum SOA concentrations exceeded 20 μg·m^{-3} and regions with high SOA shifted further north of the region (Fig. S7), which seems to closely follow the distribution of IVOC emissions (Fig. 3). Using the 1.5-D VBS scheme resulted in similar spatial pattern of simulated SOA as that of SCEN3, where regions with high SOA coincide with IVOC emissions. However, VBS led to remarkably different changes in simulated SOA concentrations from the SOAP scenarios. In contrast to the ubiquitous increase in simulated SOA in SCEN1 through SCEN3 over the BASE scenario, both increases and decreases in SOA occurred in different regions with the VBS scheme (Fig. 7). For example, in southern Anhui province and Zhejiang province, simulated SOA in SCEN4 were much lower than that of BASE scenario while the opposite trend is observed for northern YRD.

To explain this trend, we further looked at the differences in the spatial distribution of ASOA (SOA generated from anthropogenic VOC/IVOC and POA) and BSOA (SOA generated from biogenic VOC) between the BASE and SCEN4 scenario (Fig. S8). As shown by the ASOA differences, VBS led to higher ASOA concentrations because of the aging of anthropogenic VOC (for example, toluene and xylene), the inclusion of IVOC emissions, and the oxidation from POA. Increases in domain-average ASOA concentration was 0.7 μg·m^{-3} (maximum of 6.9 μg·m^{-3}). Regions with high POA emissions tended to match the large enhancement of ASOA in SCEN4. In contrast to ASOA, BSOA simulated with VBS was significantly lower over southern YRD region, where there is dense vegetation with high biogenic emissions (Liu et al., 2018) and BSOA dominated over ASOA. The large decrease in BSOA could be explained by two reasons. First, large decreases in POA and relatively smaller increases in ASOA over the southern region led to overall less available particulate mass on which BSOA could condense. Second, SOA mass yields from terpene emissions (second largest BVOC species) are lower in VBS than SOAP, which could also partially explain the reduced BSOA concentrations over regions with high BVOC emissions. Therefore, changes in SOA concentrations observed between the BASE (SOAP scheme) and SCEN4 (VBS scheme) are the combined results of changes in ASOA (pervasive increase) and BSOA (decrease over regions with high BVOC emissions).

We further compare the relative importance of ASOA and BSOA among the different scenarios (Fig. 8 and Fig. S9). For all cases, BSOA dominated over the southern YRD region due to high BVOC emissions while ASOA concentrated over the northeast YRD region. For the BASE scenario, BSOA dominated over ASOA with a domain-averaged ratio of 4 to 1, where the monthly-average ASOA concentration ($ASOA_{avg}$) was only 0.3 μg m^{-3} in the YRD region and monthly-average BSOA concentration ($BSOA_{avg}$) was 1.2 μg m^{-3}. When IVOC emissions were added, $ASOA_{avg}$ increased by 30.9–106.1%, depending on the magnitude of those emissions. Interestingly, BSOA also showed slight increases when IVOC emissions were added. This is probably because the increase of $ASOA_{avg}$ led to more BSOA entering the particulate phase. The ASOA:BSOA ratio increased from 0.3 to 0.9 when IVOC emissions were added. When SOA yields were increased by five times (SCEN3), $ASOA_{avg}$ was 1.5 μg m^{-3}, approximately five times higher than BASE scenario. Although $BSOA_{avg}$ again showed slight increases in SCEN3, $ASOA_{avg}$ exceeded $BSOA_{avg}$, suggesting comparable composition of ASOA and BSOA. In SCEN4 where the 1.5-D VBS scheme was applied, $ASOA_{avg}$ was higher by almost three times than the BASE scenario. Because $BSOA_{avg}$ was found to decrease by 11.5% compared with the BASE scenario due to reasons mentioned above, the ASOA:BSOA ratio was similar to that of SCEN3. These results have two implications. First, the formation of biogenic SOA could be affected by changes in anthropogenic emissions. Second, the magnitude of simulated SOA concentration should not be considered as the only criteria to evaluate a model's ability to simulate SOA. The relative contributions of ASOA and BSOA are also key indicators to constrain model performance. Observed SOA composition data based on SOA tracers are suitable for this purpose.

4. Conclusions

In this study, IVOC emissions for the Yangtze River Delta region were estimated based on two methods. IVOC emissions calculated by the POA method were 730 Gg with on-road and industry emissions being the dominant sources (accounting for 36.1% and 21.4%, respectively). IVOC emissions estimated by the EF method were 313 Gg, 57% less than POA method, where the major IVOC emission sources are industry (49.9%) and off-road (23.8%). IVOC emissions calculated by both methods are subject to large uncertainties (−36%–386% and 45%–610%, respectively).

Five scenarios were conducted with the CAMx photochemical model to evaluate the effects of different IVOC emissions and SOA treatments on SOA formation over the YRD region. In the BASE scenario, SOA was significantly underestimated by 61.0% at the DSL monitoring site. Adding IVOC emissions increased SOA by 7.9%–26.8%. Boosting SOA yields from IVOC by a factor of five substantially boosted simulated SOA concentrations by 135.8%. Applying the 1.5-D VBS scheme also increased SOA concentrations by 75.6% and results in highest SOA:OA ratio among all scenarios.

The distribution of ASOA and BSOA had large spatial variability, where ASOA was concentrated in the northeast of the YRD region and BSOA dominated in the southern YRD region where BVOC emissions dominate. In addition, comparison of ASOA and BSOA from different modeling scenarios showed that BSOA dominated over ASOA when the traditional SOAP scheme was used, and only when SOA yields were boosted by a factor of five did simulated ASOA concentrations exceed BSOA. In contrast, ASOA simulated by the VBS scheme was comparable with BSOA, demonstrating that credible SOA modeling methods have policy-relevant differences. Observed SOA tracer data are needed to

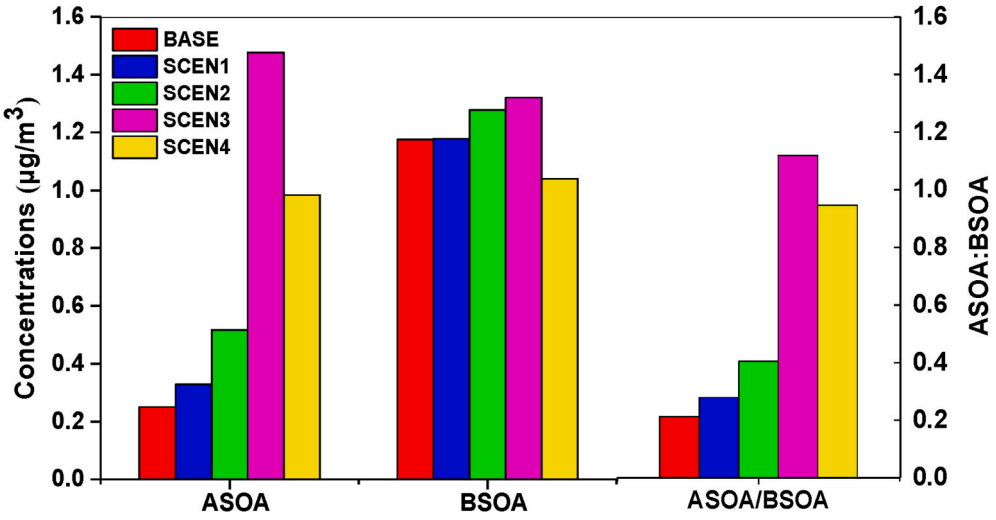

Fig. 8. Domain- and monthly-average ASOA, BSOA, and ASOA:BSOA from different modeling scenarios.

draw conclusions on which simulated SOA composition better represent reality. Nevertheless, our results show that biogenic SOA is also affected by changes in anthropogenic emissions, which has important policy implications that potentially affect further $PM_{2.5}$ reduction measures.

CRediT authorship contribution statement

Ling Huang: designed the research, performed modeling work and data analysis, wrote the paper with contributions from all co-authors. **Qian Wang:** wrote the paper with contributions from all co-authors. **Yangjun Wang:** designed the research. **Chris Emery:** reviewed and edited manuscript. **Ansheng Zhu:** helped with metrological simulation. **Yonghui Zhu:** helped with the emission inventory. **Sijia Yin:** helped with the Monte Carlo method, wrote the paper, with contributions from all co-authors. Yarwood: reviewed and edited manuscript. **Greg Yarwood:** reviewed and edited manuscript. **Li Li:** designed the research, wrote the paper with contributions from all co-authors.

Declaration of competing interest

The authors declare that they have no known competing financial interests or personal relationships that could have appeared to influence the work reported in this paper.

Acknowledgement

This study is financially sponsored by the National Natural Science Foundation of China (NO. 41105102), Shanghai Sail Program (NO. 19YF141560), the Shanghai Science and Technology Innovation Plan (NO.19DZ1205007), Shanghai International Science and Technology Cooperation Fund (NO. 19230742500), National Key R&D Program of China (NO.2018YFC0213600) and National Natural Science Foundation of China (NO. 41875161, NO. 42075144, NO. 42005112). We thank Shanghai Environmental Monitoring Center (SEMC) for conducting the measurement and sharing the data for model validation.

Appendix A. Supplementary data

Supplementary data to this article can be found online at https://doi.org/10.1016/j.atmosenv.2020.118079.

References

Chan, A.W.H., Kautzman, K.E., Chhabra, P.S., et al., 2009. Secondary organic aerosol formation from photooxidation of naphthalene and alkylnaphthalenes: implications for oxidation of intermediate volatility organic compounds (IVOCs)[J]. Atmos. Chem. Phys. 9 (9), 3049–3060.

Cao, J.J., Lee, S.C., Ho, K.F., Zou, S.C., Fung, K., Li, Y., et al., 2004. Spatial and seasonal variations of atmospheric organic carbon and elemental carbon in Pearl River Delta Region, China. Atmos. Environ. 38, 4447–4456.

Cappa, C.D., Jathar, S.H., Kleeman, M.J., et al., 2016. Simulating secondary organic aerosol in a regional air quality model using the statistical oxidation model–Part 2: assessing the influence of vapor wall losses[J]. Atmos. Chem. Phys. 16 (5), 3041–3059.

Castro, L.M., Pio, C.A., Harrison, R.M., Smith, D.J.T., 1999. Carbonaceous aerosol in urban and rural European atmospheres: estimation of secondary organic carbon concentrations. Atmos. Environ. 33, 2771–2781.

Chen, Z., Liu, J.F., Tao, W., et al., 2016. Spatio temporal distribution and source attribution of SOA in China[J]. Environ. Sci. J. Integr. Environ. Res. 37 (8), 2815–2822.

Cheng, Z., Wang, S., Fu, X., et al., 2014. Impact of biomass burning on haze pollution in the Yangtze River delta, China: a case study in summer 2011[J]. Atmos. Chem. Phys. 14 (9), 4573–4585.

Couvidat, F., Kim, Y., Sartelet, K., et al., 2013. Modeling secondary organic aerosol in an urban area: application to Paris, France[J]. Atmos. Chem. Phys. 13 (2), 983–996.

Donahue, N.M., Robinson, A.L., Pandis, S.N., 2009. Atmospheric organic particulate matter: from smoke to secondary organic aerosol[J]. Atmos. Environ. 43 (1), 94–106.

Donahue, N.M., Robinson, A.L., Stanier, C.O., et al., 2006. Coupled partitioning, dilution, and chemical aging of semivolatile organics[J]. Environ. Sci. Technol. 40 (8), 2635–2643.

Donahue, N.M., Epstein, S.A., Pandis, S.N., Robinson, A.L., 2011. A two-dimensional volatility basis set: 1. organic-aerosol mixing thermodynamics. Atmos. Chem. Phys. 11, 3303–3318.

Donahue, N.M., Kroll, J.H., Pandis, S.N., Robinson, A.L., 2012. A two-dimensional volatility basis set – Part 2: diagnostics of organic-aerosol evolution. Atmos. Chem. Phys. 12, 615–634.

Emmons, L.K., Walters, S., Hess, P.G., et al., 2010. Description and evaluation of the model for ozone and related chemical tracers, version 4 (MOZART-4)[J]. Geosci. Model Dev. (GMD) 3 (1), 43–67.

Feng, Y., Chen, Y., Guo, H., et al., 2009. Characteristics of organic and elemental carbon in PM2. 5 samples in Shanghai, China[J]. Atmos. Res. 92 (4), 434–442.

Fu, T.M., Cao, J.J., Zhang, X.Y., et al., 2011. Carbonaceous aerosols in China: top-down constraints on primary sources and estimation of secondary contribution[J]. Atmos. Chem. Phys. Discuss. 11 (10).

Gao, J., Qiao, L.P., Lou, S.R., et al., 2019. Secondary aerosol formation in urban Shanghai: insights into the roles of photochemical oxidation and aqueous-phase reaction[J]. Environ. Sci. J. Integr. Environ. Res. 40 (6), 2510–2518.

Giani, P., Balzarini, A., Pirovano, G., et al., 2019. Influence of semi-and intermediate-volatile organic compounds (S/IVOC) parameterizations, volatility distributions and aging schemes on organic aerosol modelling in winter conditions[J]. Atmos. Environ. 213, 11–24.

Guo, S., Hu, M., Zamora, M.L., et al., 2014. Elucidating severe urban haze formation in China[J]. Proc. Natl. Acad. Sci. Unit. States Am. 111 (49), 17373–17378.

Hallquist, M., Wenger, J.C., Baltensperger, U., et al., 2009. The formation, properties and impact of secondary organic aerosol: current and emerging issues[J]. Atmos. Chem. Phys. 9 (14), 5155–5236.

Han, Z., Xie, Z., Wang, G., et al., 2016. Modeling organic aerosols over east China using a volatility basis-set approach with aging mechanism in a regional air quality model [J]. Atmos. Environ. 124, 186–198.

Hayes, P.L., Carlton, A.G., Baker, K.R., et al., 2015. Modeling the formation and aging of secondary organic aerosols in Los Angeles during CalNex 2010[J]. Atmos. Chem. Phys. 15 (10), 5773–5801.

Henry, K.M., Donahue, N.M., 2012. Photochemical aging of α-pinene secondary organic aerosol: effects of OH radical sources and photolysis[J]. J. Phys. Chem. 116 (24), 5932–5940.
Hodzic, A., Jimenez, J.L., Madronich, S., et al., 2010. Modeling organic aerosols in a megacity: potential contribution of semi-volatile and intermediate volatility primary organic compounds to secondary organic aerosol formation[J]. Atmos. Chem. Phys. 10 (12), 5491–5514.
Hodzic, A., Kasibhatla, P.S., Jo, D.S., et al., 2016. Rethinking the global secondary organic aerosol (SOA) budget: stronger production, faster removal, shorter lifetime [J]. Atmos. Chem. Phys. 16 (12), 7917–7941.
Houyoux, M.R., Vukovich, J.M., Coats, C.J., et al., 2000. Emission inventory development and processing for the seasonal model for regional air quality (SMRAQ) project[J]. J. Geophys. Res.: Atmosphere 105 (D7), 9079–9090.
Huang, C., Chen, C.H., Li, L., et al., 2011. Emission inventory of anthropogenic air pollutants and VOC species in the Yangtze River Delta region, China[J]. Atmos. Chem. Phys. 11 (9), 4105.
Huang, R.J., Zhang, Y., Bozzetti, C., Ho, K.F., Cao, J.J., Han, Y., et al., 2014. High secondary aerosol contribution to particulate pollution during haze events in China. Nature 514 (7521), 218.
Jathar, S.H., Gordon, T.D., Hennigan, C.J., et al., 2014. Unspeciated organic emissions from combustion sources and their influence on the secondary organic aerosol budget in the United States[J]. Proc. Natl. Acad. Sci. Unit. States Am. 111 (29), 10473–10478.
Jathar, S.H., Woody, M., Pye, H.O.T., et al., 2017. Chemical transport model simulations of organic aerosol in southern California: model evaluation and gasoline and diesel source contributions[J]. Atmos. Chem. Phys. 17 (6), 4305–4318.
Jiang, F., Liu, Q., Huang, X., et al., 2012. Regional modeling of secondary organic aerosol over China using WRF/Chem[J]. J. Aerosol Sci. 43 (1), 57–73.
Kampa, M., Castanas, E., 2008. Human health effects of air pollution[J]. Environ. Pollut. 151 (2), 362–367.
Koo, B., Knipping, E., Yarwood, G., 2014. 1.5-Dimensional volatility basis set approach for modeling organic aerosol in CAMx and CMAQ. Atmos. Environ. 95, 158e164.
Li, J., Zhang, M., Tang, G., et al., 2019. Assessment of dicarbonyl contributions to secondary organic aerosols over China using RAMS-CMAQ[J]. Atmos. Chem. Phys. 19 (9), 6481–6495.
Li, L., Li, Q., Huang, L., et al., 2020. Air quality changes during the COVID-19 lockdown over the Yangtze River Delta Region: an insight into the impact of human activity pattern changes on air pollution variation[J]. Sci. Total Environ. 139282.
Li, M., Wang, T., Xie, M., et al., 2019. Formation and evolution mechanisms for two extreme haze episodes in the Yangtze River Delta region of China during winter 2016 [J]. J. Geophys. Res.: Atmosphere 124 (6), 3607–3623.
Liu, A., Wang, H., Cui, Y., et al., 2020. Characteristics of aerosol during a severe haze-fog episode in the Yangtze River delta: particle size distribution, chemical composition, and optical properties[J]. Atmosphere 11 (1), 56.
Liu, J., Wang, P., Zhang, H., et al., 2020. Integration of field observation and air quality modeling to characterize Beijing aerosol in different seasons[J]. Chemosphere 242, 125195.
Liu, Y., Li, L., An, J., et al., 2018. Estimation of biogenic VOC emissions and its impact on ozone formation over the Yangtze River Delta region, China[J]. Atmos. Environ. 186, 113–128.
Lannuque, V., Couvidat, F., Camredon, M., et al., 2019. Modelling organic aerosol over Europe in summer conditions with the VBS-GECKO parameterization: sensitivity to secondary organic compound properties and IVOC emissions[J]. Atmos. Chem. Phys. Discuss. https://doi.org/10.5194/acp-2018-1244 submitted for publication.
Li, J., Han, Z., Li, J., et al., 2020. The formation and evolution of secondary organic aerosol during haze events in Beijing in wintertime[J]. Sci. Total Environ. 703, 134937.
Lin, J., An, J., Qu, Y., et al., 2016. Local and distant source contributions to secondary organic aerosol in the Beijing urban area in summer[J]. Atmos. Environ. 124, 176–185.
Liu, H., Man, H., Cui, H., et al., 2017. An updated emission inventory of vehicular VOCs and IVOCs in China[J]. Atmos. Chem. Phys. 17 (20), 12709.
Liu, J., Shen, J., Cheng, Z., et al., 2020. Source apportionment and regional transport of anthropogenic secondary organic aerosol during winter pollution periods in the Yangtze River Delta, China[J]. Sci. Total Environ. 710, 135620.
Liu, Y., Jia, R., Dai, T., et al., 2014. A review of aerosol optical properties and radiative effects[J]. Journal of Meteorological Research 28 (6), 1003–1028.
Lu, B., Huang, C., Lu, Q., et al., 2018. Emission inventory and pollution characteristics of industrial VOCs in Hangzhou , China[J]. Environ. Sci. J. Integr. Environ. Res. 39 (2), 533–542.
Ma, P.K., Zhao, Y., Robinson, A.L., et al., 2017. Evaluating the impact of new observational constraints on PS/IVOC emissions, multi-generation oxidation, and chamber wall losses on SOA modeling for Los Angeles, CA[J]. Atmos. Chem. Phys. 17 (15), 9237–9259.
Meroni, A., Pirovano, G., Gilardoni, S., et al., 2017. Investigating the role of chemical and physical processes on organic aerosol modelling with CAMx in the Po Valley during a winter episode[J]. Atmos. Environ. 171, 126–142.
Murphy, B.N., Woody, M.C., Jimenez, J.L., et al., 2017. Semivolatile POA and parameterized total combustion SOA in CMAQv5.2: impacts on source strength and partitioning[J]. Atmos. Chem. Phys. 17. PNNL-SA-124491.
Murphy, D.M., Cziczo, D.J., Froyd, K.D., et al., 2006. Single-particle mass spectrometry of tropospheric aerosol particles[J]. J. Geophys. Res.: Atmosphere 111 (D23).
Nenes, A., Pilinis, C., Pandis, S.N., 1998. ISORROPIA: a new thermodynamic model for multiphase multicomponent inorganic aerosols. Aquat. Geochem. 4, 123–152.
Odum, J.R., Hoffmann, T., Bowman, F., et al., 1996. Gas/particle partitioning and secondary organic aerosol yields[J]. Environ. Sci. Technol. 30 (8), 2580–2585.
Presto, A.A., Miracolo, M.A., Donahue, N.M., et al., 2010. Secondary organic aerosol formation from high-NOx photo-oxidation of low volatility precursors: n-alkanes[J]. Environ. Sci. Technol. 44 (6), 2029–2034.
Pui, D.Y.H., Chen, S.C., Zuo, Z., 2014. $PM_{2.5}$ in China: measurements, sources, visibility and health effects, and mitigation[J]. Particuology 13, 1–26.
Qi, L., Liu, H., Shen, X., et al., 2019. Intermediate-volatility organic compound emissions from nonroad construction machinery under different operation modes[J]. Environ. Sci. Technol. 53 (23), 13832–13840.
Ramboll, 2018. CAMx (Comprehensive Air Quality Model with Extensions) User's Guide. Version 6.5. www.camx.com.
Robinson, A.L., Donahue, N.M., Shrivastava, M.K., et al., 2007. Rethinking organic aerosols: semivolatile emissions and photochemical aging[J]. Science 315 (5816), 1259–1262.
Strader, R., Lurmann, F., Pandis, S.N., 1999. Evaluation of secondary organic aerosol formation in winter[J]. Atmos. Environ. 33 (29), 4849–4863.
Stockwell, C.E., Veres, P.R., Williams, J., et al., 2015. Characterization of biomass burning emissions from cooking fires, peat, crop residue, and other fuels with high-resolution proton-transfer-reaction time-of-flight mass spectrometry[J]. Atmos. Chem. Phys. 15 (2), 845–865.
Sun, X.B., Liao, C.H., Zeng, W.T., et al., 2018. Emission inventory of atmospheric pollutants and VOC species from crop residue burning in Guangdong province[J]. Environ. Sci. J. Integr. Environ. Res. 39 (9), 3995–4001.
Sun, P., Nie, W., Wang, T., et al., 2020. Impact of air transport and secondary formation on haze pollution in the Yangtze River Delta: in situ online observations in Shanghai and Nanjing[J]. Atmos. Environ., 117350
Sun, Y., Wang, Z., Wild, O., et al., 2016. "APEC blue": secondary aerosol reductions from emission controls in Beijing[J]. Sci. Rep. 6, 20668.
Sun, Y., Du, W., Fu, P., Wang, Q., Li, J., Ge, X., et al., 2016. Primary and secondary aerosols in Beijing in winter: sources, variations and processes. Atmos. Chem. Phys. 16 (13), 8309–8329.
Tkacik, D.S., Presto, A.A., Donahue, N.M., et al., 2012. Secondary organic aerosol formation from intermediate-volatility organic compounds: cyclic, linear, and branched alkanes[J]. Environ. Sci. Technol. 46 (16), 8773–8781.
Woody, M.C., Baker, K.R., Hayes, P.L., et al., 2016. Understanding sources of organic aerosol during CalNex-2010 using the CMAQ-VBS[J]. Atmos. Chem. Phys. 16 (6), 4081–4100.
Woody, M.C., West, J.J., Jathar, S.H., et al., 2014. Estimates of non-traditional secondary organic aerosols from aircraft SVOC and IVOC emissions using CMAQ[J]. ACPD 14 (22), 30667–30703.
Wu, L., Wang, X., Lu, S., et al., 2019. Emission inventory of semi-volatile and intermediate-volatility organic compounds and their effects on secondary organic aerosol over the Pearl River Delta region[J]. Atmos. Chem. Phys. 19 (12), 8141–8161.
Xia, S.J., Liu, Q., Zhao, Q.Y., 2018. Emission inventory of anthropogenically sourced VOCs and its contribution to ozone formation in Jiangsu province[J]. Environ. Sci. J. Integr. Environ. Res. 39 (2), 592–599.
Xie, Y.B., Chen, J., Li, W., 2014. An assessment of PM2. 5 related health risks and impaired values of Beijing residents in a consecutive high-level exposure during heavy haze days[J]. Environ. Sci. J. Integr. Environ. Res. 35 (1), 1–8.
Xu, J., Wang, Q., Deng, C., et al., 2018. Insights into the characteristics and sources of primary and secondary organic carbon: high time resolution observation in urban Shanghai[J]. Environ. Pollut. 233, 1177–1187.
Xu, Z., Wen, T., Li, X., et al., 2015. Characteristics of carbonaceous aerosols in Beijing based on two–year observation[J]. Atmospheric Pollution Research 6 (2), 202–208.
Yao, T., Li, Y., Gao, J., et al., 2020. Source apportionment of secondary organic aerosols in the Pearl River Delta region: contribution from the oxidation of semi-volatile and intermediate volatility primary organic aerosols[J]. Atmos. Environ. 222, 117111.
Yarwood, G., Jung, J., Whitten, G.Z., Heo, G., Mellberg, J., Estes, E., 2010. Updates to the carbon Bond mechanism for version 6 (CB6). Chapel Hill, October. Presented at the 9th Annual CMAS Conference.
Zhang, C., Lu, X., Zhai, J., et al., 2018. Insights into the formation of secondary organic carbon in the summertime in urban Shanghai[J]. J. Environ. Sci. 72, 118–132.
Zhang, Q., Jimenez, J.L., Canagaratna, M.R., et al., 2007. Ubiquity and dominance of oxygenated species in organic aerosols in anthropogenically-influenced Northern Hemisphere midlatitudes[J]. Geophys. Res. Lett. 34 (13).
Zhang, L., Brook, J.R., Vet, R., 2003. A revised parameterization for gaseous dry deposition in air-quality models. Atmos. Chem. Phys. 3, 2067–2082.
Zhao, B., Wang, S., Donahue, N.M., et al., 2016a. Quantifying the effect of organic aerosol aging and intermediate-volatility emissions on regional-scale aerosol pollution in China[J]. Sci. Rep. 6 (1), 1–10.
Zhao, Y., Nguyen, N.T., Presto, A.A., et al., 2015. Intermediate volatility organic compound emissions from on-road diesel vehicles: chemical composition, emission factors, and estimated secondary organic aerosol production[J]. Environ. Sci. Technol. 49 (19), 11516–11526.
Zhao, Y., Nguyen, N.T., Presto, A.A., et al., 2016b. Intermediate volatility organic compound emissions from on-road gasoline vehicles and small off-road gasoline engines[J]. Environ. Sci. Technol. 50 (8), 4554–4563.
Zheng, M., Yan, C.Q., Li, X.Y., et al., 2014. A review of methods for quantifying secondary organic aerosol[J]. China Environ. Sci. 34 (3), 555–564.